ARTICLE

Cross-Propagation Sum-Frequency Generation Vibrational Spectroscopy†

Li Fu[a], Shun-li Chen[a,b], Wei Gan[b], Hong-fei Wang[a]*

a. William R. Wiley Environmental Molecular Sciences Laboratory, Pacific Northwest National Laboratory, 902 Battelle Boulevard, P.O. Box 999, Richland, WA 99352, USA
b. Laboratory of Environmental Science and Technology, Xinjiang Technical Institute of Physics Chemistry, Key Laboratory of Functional Materials and Devices for Special Environments, Chinese Academy of Sciences, Urumqi 830011, China

(Dated: Received on December 2, 2015; Accepted on December 28, 2015)

Here we report the theory formulation and the experiment realization of sum-frequency generation vibrational spectroscopy (SFG-VS) in the cross-propagation (XP) geometry or configuration. In the XP-SFG-VS, the visible and the infrared (IR) beams in the SFG experiment are delivered to the same location on the surface from visible and IR incident planes perpendicular to each other, avoiding the requirement to have windows or optics to be transparent to both the visible and IR frequencies. Therefore, the XP geometry is applicable to study surfaces in the enclosed vacuum or high pressure chambers with far infrared (FIR) frequencies that can directly access the metal oxide and other lower frequency surface modes, with much broader selection of visible and IR transparent window materials. The potential applications include surface science, material science, fundamental catalytic sciences, as well as low temperature molecular sciences, *etc.*

Key words: Sum-frequency generation, Vibrational spectroscopy, Co-propagation, Counter-propagation, Cross-propagation

I. INTRODUCTION

Surface sum-frequency generation vibrational spectroscopy (SFG-VS), first developed three decades ago [1], has shown great promises in study of all kinds of surfaces and interfaces as a unique spectroscopic tool with its surface specificity and sub-monolayer sensitivity [2–8]. Many recent developments aiming to quantitative measurement and interpretation of SFG-VS data from complex molecular interfaces have focused on the aspects of the spectral phase, polarization and spectral resolution [9–12]. Among these developments, the issues on polarization [10] and spectral resolution [12–14] have been less controversial, and the controversies regarding the issues on the consistency [9, 15, 16] between the phase-resolved and intensity SFG-VS spectra measurements are also converging recently [14, 17, 18].

In the SFG-VS experiment, a visible laser beam (ω_1), and a tunable or broadband infrared (IR) laser beam (ω_2) in the mid-IR (3−8 μm) or long-IR (8−15 μm) frequency range are focused simultaneously onto the surface or interface of interest, and a weak signal at the sum of the two frequencies (ω=ω_1+ω_2) is generated. By fixing the visible frequency, usually at 532 or 800 nm, and tuning the IR frequency, the vibrational spectroscopy of the surface or interfacial molecules can be detected, to provide the spectroscopy, structure, conformation and dynamics information of the molecular species of interest. The unique surface selectivity of SFG-VS comes from the intrinsic symmetry requirement for the second-order nonlinear process which is forbidden for the centrosymmetric medium and the fact that the centrosymmetry of any surface or interface is always broken [19, 20]. The practical considerations in the actual SFG-VS experiment are usually on what is the best way for the visible and IR light to be accessible to the surface or interface of interest, and on whether enough SFG signal can be generated and detected under specific polarization and spectral resolution, *etc.*

In the SFG-VS literature, so far almost all SFG-VS experiment has been performed using the co-planar geometry (Fig.1), either in the reflective or transmission modes with co-propagation, counter-propagation or two-phase propagation arrangements of the visible and IR beams [5, 7, 21–24]. In the co-planar geometry, the visible and IR beam are all within the same incident plane that is perpendicular to the surface or interface. It is clear that for the exposed surfaces, there is no problem for the visible and IR beams to access the surface, and the detection of SFG signal can be either reflective or refractive. For the refractive detection, the only requirement is that the lower phase is transmissible for the SFG signal. For the buried interface, the issues, on

†Part of the special issue for "the Chinese Chemical Society's 14th National Chemical Dynamics Symposium".
*Author to whom correspondence should be addressed. E-mail: hongfei.wang@pnnl.gov, Tel.: +1-509-371-6717, FAX: +1-509-371-6445

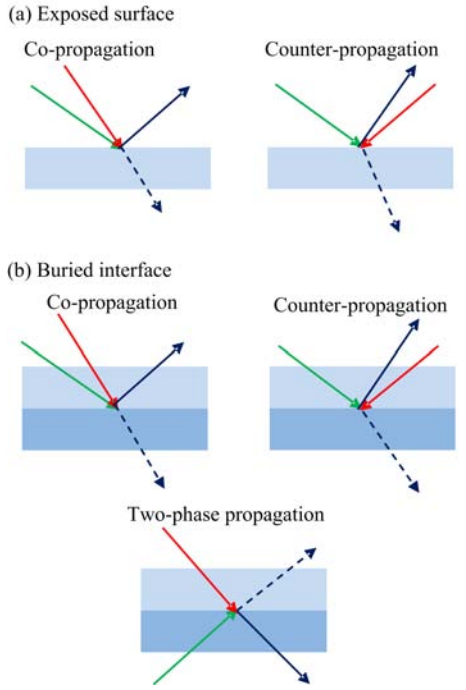

FIG. 1 Typical SFG-VS with co-planar geometry for exposed surfaces and buried interfaces. The visible, IR, SFG signal in the reflective and refractive detection are represented by the green solid, red solid, blue solid and blue dashed lines, respectively.

whether either of the upper or lower phase is transmissible for the visible or IR light to allow them to access the interface and to allow the SFG signal in the visible to be detected, always have to be evaluated in the SFG-VS experiment. So, all three geometries for the buried interfaces work only when the upper phase is IR transmissible, either transparent to the IR frequencies of interest or thin enough to allow insignificant absorption for the IR frequencies. This is why even though there have been successful cases for SFG-VS measurement of molecules and nanoparticles at buried interfaces [24–28], the application of SFG-VS to buried interfaces are still challenging and limited [29].

In this work, we present the formulation and experiment validation of the SFG-VS in a non-co-planar geometry, *i.e.* the cross-propagation (XP) geometry, in which the incident planes of the visible and IR beams are perpendicular to each other, and they are both perpendicular to the surface. As far as we have known, SFG-VS measurement under such geometry has not been reported in the literature. In the XP geometry, the visible and IR are delivered to the surface sharing no common optics. Therefore, the advantage of the XP geometry is that there is no requirement of the optical element to be transparent for both the visible and IR light. The XP geometry is not really useful for the application to buried interface measurement, but it can be useful for the applications to the exposed surface enclosed in a vacuum or pressure chamber for surface science and fundamental catalysis studies [4, 5, 30–33], where transparent optical windows for the visible and IR lights are needed. In the co-planar geometry, either co-propagation or counter-propagation, at least one window needs to be transparent for both the visible and IR beams. Such requirement significantly narrows the choices of suitable optical window materials that are both robust and stable. For example, CaF_2 window allows transmission of the visible frequency and IR frequency above 1000 cm^{-1}, and BaF_2 windows allow transmission of visible frequencies and IR frequency above ∼650 cm^{-1}. But both materials are known to be brittle and not quite robust or stable for vacuum and pressure chambers. While KBr or CsI windows allow transmission of the visible frequencies and the IR frequency down to 300 cm^{-1}(KBr) or even 200 cm^{-1}(CsI), these windows are known to be easily degradable under moisture. Since with the XP-geometry the visible and IR beams no longer pass through the same windows, the above-mentioned limitations on the choice of the window materials are removed.

In the following section, as the XP-SFG-VS has not been reported before, we first present the formulation of the XP-SFG-VS and the derivation of the experimental measurable properties similar to the formulations as in the most commonly used co-propagation geometry as in the SFG-VS literatures [10, 11, 34, 35]; then we present experimental results using the XP-SFG-VS measurement on the air/DMSO (dimethyl sulfoxide) interface, cyclohexanol on the vapor/z-cut α-quartz surface in the C−H stretching vibration region, *i.e.* in 2800−3050 cm^{-1}, and the air/z-cut α-quartz surface in the 1000−1280 cm^{-1} phonon mode region. These experimental results provided verification on the effectiveness of the formulations. With these established, vacuum and pressure chambers for XP-SFG-VS can be designed and constructed accordingly for surface science and fundamental catalysis studies with extended IR frequency range.

II. THEORY FORMULATION OF CROSS-PROPAGATION GEOMETRY

Here we present the formulations of the effective susceptibility terms for the cross-propagation SFG-VS, *i.e.* XP-SFG-VS of the rotationally isotropic surface with the C_∞ symmetry, and the z-cut α-quartz surfaces with the D_3 symmetry. Other important crystal surfaces with different symmetries, such as the anatase or rutile TiO_2 surfaces, can be formulated similarly. In these formulation, the optical field needs to be projected to the principal axes in the laboratory coordinates system and proper products of the optical fields and the macroscopic susceptibility tensors of the surface need to be obtained.

DOI:10.1063/1674-0068/29/cjcp1512248

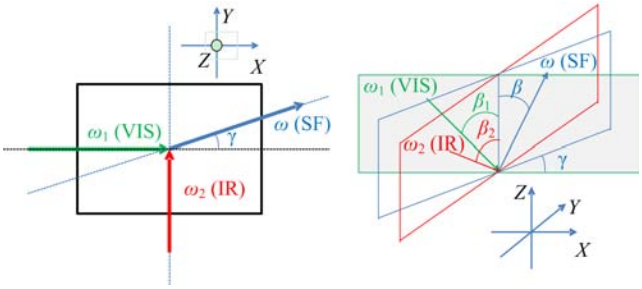

FIG. 2 Illustration of the vector and field projection relationship in XP-SFG-VS in the laboratory coordinates system (X, Y, Z). On the left is the top view on the projection to the XY plane, and on the right is the side view facing the visible incident plane, *i.e.* the XZ plane.

A. The SFG detection angles in the XP-SFG-VS

Figure 2 shows the wave vector and field directions of the visible, the IR and the SFG signal fields in the XP-SFG-VS. Here, the incoming visible beam (ω_1) is in the XZ plane with an incident angle of β_1 from the surface normal z; the incoming IR beam (ω_2) is in the YZ plane with an incident angle β_2; and the outgoing SFG beam (ω) is in a plane that is with an dihedral angle of γ from the XZ plane with the outgoing angle of β from the surface normal z. In co-planar geometry, as in Fig.1, the visible, IR and SFG signal beams are all in the same incident plane. However, in the XP-SFG-VS shown in Fig.2, neither two of the three beams are in the same incident plane. Accordingly, the wave vector projections of the visible, IR and SFG beams are listed in the Table I.

Since in the SFG process the wave vectors of the visible, IR and SFG beams should satisfy both the energy conservation condition and the momentum conservation condition in both the X and Y directions [36, 37], one has, for energy conservation:

$$\omega = \omega_1 + \omega_2 \tag{1}$$

for momentum conservation:

$$\omega_1 \sin\beta_1 = \omega \sin\beta \cos\gamma \tag{2}$$

$$\omega_2 \sin\beta_2 = \omega \sin\beta \sin\gamma \tag{3}$$

The momentum conservation condition in the XP-SFG-VS is related to two angles, *i.e.* β and γ. In comparison, the momentum conservation condition in the co-planar geometry is only related to one outgoing angle β [10, 11, 35]. Thus, when β_1=β_2,

$$\tan\gamma = \frac{\omega_2 \sin\beta_2}{\omega_1 \sin\beta_1} = \frac{\omega_2}{\omega_1} \tag{4}$$

$$\sin\beta = \frac{\omega_1 \sin\beta_1}{\omega \cos\left(\arctan\dfrac{\omega_2 \sin\beta_2}{\omega_1 \sin\beta_1}\right)}$$

TABLE I Wave vector projection in Fig.2.

	SF	VIS	IR
$\hat{X}$	$\sin\beta\cos\gamma$	$\sin\beta_1$	0
$\hat{Y}$	$\sin\beta\sin\gamma$	0	$\sin\beta_2$
$\hat{Z}$	$\cos\beta$	$\cos\beta_1$	$\cos\beta_2$

$$= \frac{\omega_1 \sin\beta_1}{\omega \cos\left(\arctan\dfrac{\omega_2}{\omega_1}\right)} \tag{5}$$

Eq.(4) and Eq.(5) defines the unique outgoing direction of the SFG signal from the values of the frequencies and incident angles of the visible and IR beams. One can see that the relationships in Eq.(4) and Eq.(5) are simplified when the visible and IR incident angles are equal, *i.e.* β_1=β_2. Since now the visible and IR beams are in XZ and YZ planes, respectively, β_1=β_2 is apparently different from the case of collinear propagation condition in the co-propagation case with the co-planar geometry.

Using Eq.(4) and Eq.(5), one can calculate the β and the γ values for the typical SFG experiment with visible beam wavelength at 800 or 532.1 nm, and different IR frequencies. These results for the typical β and γ values of the simplified case with β_1=β_2 are listed in the Table II. β and γ values for the more general cases with $\beta_1 \neq \beta_2$ can also be directly calculated from the Eq.(4) and Eq.(5). One can see from Table II that the dihedral angle γ values change in the range of 15° with 800 nm visible and IR in the full range of 300−4000 cm^{-1}, and are about 11° with 532.1 nm visible and IR in the full range of 300−4000 cm^{-1}. Such results also indicate that in a typical SFG experiment with IR frequency changing in the range of 300 cm^{-1}, the γ angle for SFG signal detection is usually within 1° or so. The same is true for the outgoing angle β. For such a small change of the β and γ values, there is generally no need to vary the detection angle in a typical XP-SFG-VS experiment. However, if the IR range is much larger than 300 cm^{-1}, some adjustment of the β and γ angles is necessary.

B. The field projections in the XP-SFG-VS

In order to know the SFG signal in different polarizations, the polarizations and the projections of the visible, the IR and the SFG signal fields in the laboratory coordinates system (X, Y, Z) need to be known (Table III). In Table III, the polarization s is defined as the field direction that is perpendicular to the incident (for visible and IR beams) or outgoing (for SFG signal beam) plane, and the polarization p is defined as the field direction is in the incident or outgoing plane. One can see that the s and p polarizations for the visible, the IR and the SFG signal beams are all different. For example, the s polarization of the visible beam is along

DOI:10.1063/1674-0068/29/cjcp1512248

TABLE II Some incident and outgoing angles in cross-propagation geometry with β_1=β_2.

$\omega_1/\mathrm{cm}^{-1}$	$\omega_2/\mathrm{cm}^{-1}$	ω/cm^{-1}	$\gamma/(^\circ)$	$\sin\beta/\sin\beta_1$	$\beta/(^\circ)$		
					β_1=65°	β_1=55°	β_1=45°
12500	300	12800	1.4	0.98	62.3	53.1	43.7
(800 nm)	600	13100	2.7	0.96	60.0	51.5	42.5
	1000	13500	4.6	0.93	57.3	49.6	41.1
	1200	13700	5.5	0.92	56.5	48.9	40.6
	1800	14300	8.2	0.88	52.9	46.1	38.5
	2800	15300	12.6	0.84	49.6	43.5	36.4
	3000	15500	13.5	0.83	48.8	42.8	35.9
	4000	16500	17.7	0.80	35.2	40.9	34.4
18794	300	19094	0.9	0.98	63.1	53.7	44.1
(532.1 nm)	600	19394	1.8	0.97	61.5	52.6	43.3
	1000	19794	3.0	0.95	59.5	51.1	42.2
	1200	19994	3.7	0.94	58.4	50.4	41.7
	1800	20594	5.5	0.92	56.5	48.9	40.6
	2800	21594	8.5	0.88	52.9	46.1	38.5
	3000	21794	9.1	0.87	52.0	45.5	38.0
	4000	22794	12.0	0.84	49.6	43.5	36.4

TABLE III Some incident and outgoing angles in cross-propagation geometry with β_1=β_2.

	SF			VIS			IR		
	All	s	p	All	s	p	All	s	p
$\hat{X}$	$-(\cos\Omega\cos\beta\cos\gamma+\sin\Omega\sin\gamma)$	$-\sin\gamma$	$-\cos\beta\cos\gamma$	$\cos\Omega_1\cos\beta_1$	0	$\cos\beta_1$	$\sin\Omega_2$	1	0
$\hat{Y}$	$-\cos\Omega\cos\beta\sin\gamma+\sin\Omega\cos\gamma$	$\cos\gamma$	$-\cos\beta\sin\gamma$	$\sin\Omega_1$	1	0	$\cos\Omega_2\cos\beta_2$	0	$\cos\beta_2$
$\hat{Z}$	$\cos\Omega\sin\beta$	0	$\sin\beta$	$\cos\Omega_1\sin\beta_1$	0	$\sin\beta_1$	$\cos\Omega_2\sin\beta_2$	0	$\sin\beta_2$

the Y direction in the laboratory frame, while the s polarization of the IR beam is along the X direction. This cross relationship between the visible and the IR beams is the direct result of the cross-propagation geometry. If the incident plane of the visible and the IR beams are not perpendicular to each other, the vector projection and the filed projection relationships can also be derived, but they are to be more complicated. In this study, we stick to the simplest case with these two incident planes perpendicular to each other as defined in Fig.1.

Using the polarization definition and the projection of the three laser optical beams, one can directly derive the SFG tensor element expressions by knowing the macroscopic susceptibility tensors of the surfaces. The relationships between the non-zero elements of the macroscopic susceptibility tensor elements of the surface are different for surfaces with different symmetry properties. Below the results for the rotationally isotopic surface (C_∞ symmetry) and the z-cut α-quartz surface (D_3 symmetry) are presented.

C. Expressions for the rotationally isotropic surface (C_∞ symmetry)

The rotationally isotropic surface (C_∞), has 11 non-zero elements (7 achiral and 4 chiral) as the followings [7, 11], for Achiral terms:

$$ZZZ, XXZ = YYZ, XZX = YZY, ZXX = ZYY \quad (6)$$

for chiral terms:

$$XYZ = -YXZ, \quad XZY = -YZX \quad (7)$$

For an achiral rotationally isotropic surface (C_∞ symmetry), only the 7 achiral terms are non-zero. The complete non zero elements in different polarization combinations are listed in the Table IV. The terms in red are the achiral susceptibility tensors and the terms in black are the chiral susceptibility tensors.

Therefore, using the definition of the s and p polarization for the visible, the IR and the SFG signal beams in Table III, the effective susceptibility terms that can be directly measured in the XP-SFG-VS experiment with

DOI:10.1063/1674-0068/29/cjcp1512248

TABLE IV Elements and non-zero elements for cross-propagation geometry.

Polarization combinations	All elements	Non-zero elements	
		C_∞	D_3 rotating around z-axis
sss	XYX, YYX		XYX, YYX
ssp	XYY, XYZ, YYY, YYZ	XYZ, YYZ	XYY, XYZ, YYY
sps	XXX, XZX, YXX, YZX	XZX, YZX	XXX, YXX, YZX
pss	XYX, YYX, ZYX	ZYX	XYX, YYX
pps	$XXX, XZX,$	XZX	XXX
	$YXX, YZX,$	YZX	YXX, YZX
	ZXX, ZZX	ZXX	
psp	XYY, XYZ	XYZ	XYY, XYZ
	YYY, YYZ	YYZ	YYY
	ZYY, ZYZ	ZYY	
spp	XXY, XZY, XXZ, XZZ	XZY, XXZ	XXY
	YXY, YZY, YXZ, YZZ	YZY, YXZ	YXY, YXZ
ppp	XXY, XZY, XXZ, XZZ	XZY, XXZ	XXY, XZY
	YXY, YXZ, YZY, YZZ	YXZ, YZY	YXY, YXZ
	ZXY, ZZY, ZXZ, ZZZ	ZXY, ZZZ	

eight polarization combinations are derived and listed in Eq.(8)−(14) below.

$$\chi_{sss}=0 \tag{8}$$

$$\chi_{ssp}=L_{YY}(\omega)L_{YY}(\omega_1)L_{ZZ}(\omega_2)\cos\gamma\sin\beta_2\cdot\chi_{YYZ}-L_{XX}(\omega)L_{YY}(\omega_1)L_{ZZ}(\omega_2)\sin\gamma\sin\beta_2\cdot\chi_{XYZ}$$

$$\chi_{sps}=-L_{XX}(\omega)L_{ZZ}(\omega_1)L_{YY}(\omega_2)\sin\gamma\sin\beta_1\cdot\chi_{XZX}+L_{YY}(\omega)L_{ZZ}(\omega_1)L_{YY}(\omega_2)\cos\gamma\sin\beta_1\cdot\chi_{YZX} \tag{9}$$

$$\chi_{pss}=L_{ZZ}(\omega)L_{YY}(\omega_1)L_{YY}(\omega_2)\sin\beta\cdot\chi_{ZYX} \tag{10}$$

$$\chi_{pps}=-L_{XX}(\omega)L_{ZZ}(\omega_1)L_{YY}(\omega_2)\cos\gamma\cos\beta\sin\beta_1\cdot\chi_{XZX}-L_{YY}(\omega)L_{ZZ}(\omega_1)L_{YY}(\omega_2)\sin\gamma\cos\beta\cdot\sin\beta_1\chi_{YZX}+L_{ZZ}(\omega)L_{XX}(\omega_1)L_{YY}(\omega_2)\cdot\sin\beta\cos\beta_1\cdot\chi_{ZXX} \tag{11}$$

$$\chi_{psp}=-L_{XX}(\omega)L_{YY}(\omega_1)L_{ZZ}(\omega_2)\cos\gamma\cos\beta\sin\beta_2\cdot\chi_{XYZ}-L_{YY}(\omega)L_{YY}(\omega_1)L_{ZZ}(\omega_2)\sin\gamma\cos\beta\cdot\sin\beta_2\chi_{YYZ}+L_{ZZ}(\omega)L_{YY}(\omega_1)L_{XX}(\omega_2)\sin\beta\cos\beta_2\cdot\chi_{ZYY} \tag{12}$$

$$\chi_{spp}=-L_{XX}(\omega)L_{ZZ}(\omega_1)L_{XX}(\omega_2)\sin\gamma\sin\beta_1\cos\beta_2\cdot\chi_{XZY}-L_{XX}(\omega)L_{XX}(\omega_1)L_{ZZ}(\omega_2)\sin\gamma\cdot\cos\beta_1\sin\beta_2\cdot\chi_{XXZ}+L_{YY}(\omega)L_{ZZ}(\omega_1)\cdot L_{XX}(\omega_2)\cos\gamma\sin\beta_1\cos\beta_2\cdot\chi_{YZY}+L_{YY}(\omega)L_{XX}(\omega_1)L_{ZZ}(\omega_2)\cos\gamma\cdot\cos\beta_1\sin\beta_2\cdot\chi_{YXZ} \tag{13}$$

$$\chi_{ppp}=-L_{XX}(\omega)L_{XX}(\omega_1)L_{ZZ}(\omega_2)\cos\gamma\cos\beta\cos\beta_1\cdot\sin\beta_2\cdot\chi_{XXZ}-L_{XX}(\omega)L_{ZZ}(\omega_1)L_{XX}(\omega_2)\cdot\cos\gamma\cos\beta\sin\beta_1\cos\beta_2\cdot\chi_{XZY}-L_{YY}(\omega)\cdot L_{XX}(\omega_1)L_{ZZ}(\omega_2)\sin\gamma\cos\beta\cos\beta_1\sin\beta_2\cdot\chi_{YXZ}-L_{YY}(\omega)L_{ZZ}(\omega_1)L_{XX}(\omega_2)\sin\gamma\cdot\cos\beta\cdot\sin\beta_1\cos\beta_2\cdot\chi_{YZY}+L_{ZZ}(\omega)\cdot L_{XX}(\omega_1)L_{XX}(\omega_2)\sin\beta\cos\beta_1\cos\beta_2\cdot\chi_{ZXY}+L_{ZZ}(\omega)L_{ZZ}(\omega_1)L_{ZZ}(\omega_2)\cdot\sin\beta sin\beta_1\sin\beta_2\cdot\chi_{ZZZ} \tag{14}$$

In these expressions, the red terms are the achiral terms and the black terms are the chiral terms, and the $L_{II}(\omega_i)$ are the SFG Fresnel factors defined in the SFG literature [11, 35]. It is to be noted that for SFG Fresnel factors, since the IR beam is in the cross geometry from the visible incident plane, the expressions of $L_{XX}(\omega_2)$ and $L_{YY}(\omega_2)$ terms for the IR beam should exchange their positions with each other, as the XZ plane is defined as the incident plane in obtaining the Fresnel factors, while in the cross-geometry case the YZ plane is the incident plane for the IR beam. For VIS and SF beam, the definition is still the same as in the literature [11, 35].

It is interesting to see that for the C_∞ surface, all the 7 non-zero polarization combinationterms, *i.e.* ssp, sps, pss, pps, psp, spp, and ppp, are not purely achiral. In contrast, in the co-planar geometry, the ssp, sps, pss and ppp terms are always purely achiral [7, 11]. In the co-planar geometry, the ssp, sps, pss terms are all function of a single achiral macroscopic susceptibility tensors, *i.e.* YYZ, YZY, and ZYY, respectively [7, 11]. However, in the XP-SFG-VS, only the pss term is a function of a single chiral term ZYX (Eq.(10)). Therefore, the polarization combination terms in the XP-SFG-VS are generally more complicated than the corresponding polarization combination terms. This is probably the principal reason that as far as we have known, there has been no study with XP-SFG-VS geometry in the SFG-VS literature.

DOI:10.1063/1674-0068/29/cjcp1512248

However, a closer examination of all the polarization combination terms in Eq.(8) to Eq.(14) shows that these terms are not so difficult to understand or measure, and they can be simplified or reduced to simple terms with good approximation. For example, for a given molecular surface, the achiral YYZ term is usually larger than the chiral XYZ term, and also in the XP-SFG-VS experiment $\cos\gamma$ is usually much larger than $\sin\gamma$, because γ is usually a small angle (see Table II). This is particularly true when at lower IR frequencies such as 300 or 600 cm^{-1}, the range that the XP-SFG-VS geometry is most useful in avoiding the limitation of the selection for window materials. Consequently, the contribution from the chiral XYZ term in the ssp polarization combination in XP-SFG-VS (Eq.(9)) is usually much smaller or even negligible in comparison with the contribution of the achiral YYZ term. Thus, the ssp term can basically be approximated by the single achiral YYZ term, making the ssp polarization term in the XP-SFG-VS similar to the ssp polarization term in the co-planar geometry. The rest of the terms in the Eq.(8) to Eq.(14) can also be evaluated in the same way. And it is easy to show that despite the differences in their expressions, qualitatively speaking, the polarization terms in the XP-SFG-VS are usually dominated by the same polarization terms in the co-planar geometry measurement. Of course, detailed quantitative analysis of the XP-SFG-VS data will show the differences from the co-planar geometry measurements. Nevertheless, qualitative understanding of the XP-SFG-VS data is not as difficult as the above expressions seemingly imply.

D. Expressions for z-cut α-quartz surface (D_3 symmetry)

The non-zero macroscopic susceptibility tensors of the z-cut α-quartz are listed in the Table IV. There are eight achiral elements and 6 chiral elements. In order to get the complete expressions of XP-SFG-VS polarization terms for the z-cut α-quartz surface, one needs to consider the azimuthal angle dependences, *i.e.* rotational dependence along the z axis of the z-cut α-quartz crystal. In order to do this, one has to consider the non-zero polarizability tensors of the unit cell of the quartz crystal with D_3 group symmetry. There are 8 non-zero polarizability elements (4 achiral and 4 chiral) for the unit cell of the quartz crystal, with the unit cell coordinates system defined as (x, y, z) [38], *i.e.*,
for achiral terms:

$$xxx = -xyy = -yzy = -yyz \tag{15}$$

for chiral terms:

$$xyz = xzy = -yzx = -yxz \tag{16}$$

Also it is known that for the left-handed α-quartz, $xxx/xyz>0$, while for the right-handed α-quartz $xxx/xyz<0$ [38]. For z-cut quartz, the transformation matrix for rotation around the z-axis with the azimuthal angle ϕ placed in the Z direction of the laboratory coordinates system (X, Y, Z) (Fig.3) is,

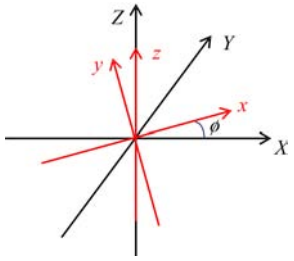

FIG. 3 Definition of the z-cut α-quartz crystal rotation against laboratory frame.

TABLE V Non-zero macroscopic terms for z-cut quartz crystal in terms of the microscopic polarizability tensor terms of the unit cell.

Elements of $\chi^{(2)}$ probed in laboratory frame	Transformation of $\chi^{(2)}$ red terms from sample into laboratory frame
YYY	$-\beta_{xxx}\sin 3\phi$
YYX	$-\beta_{xxx}\cos 3\phi$
YXY	$-\beta_{xxx}\cos 3\phi$
YXX	$\beta_{xxx}\sin 3\phi$
YZX	$-\beta_{xyz}$
YXZ	$-\beta_{xyz}$
XYY	$-\beta_{xxx}\cos 3\phi$
XYX	$\beta_{xxx}\sin 3\phi$
XYZ	β_{xyz}
XXY	$\beta_{xyz}\sin 3\phi$
XZY	β_{xyz}
XXX	$\beta_{xxx}\cos 3\phi$

* Red terms are for macroscopic D_3 symmetry when achiral terms are dominant.
** Black terms are for macroscopic D_3 symmetry when achiral terms are dominant.

$$R = \begin{pmatrix} R_{xx} & R_{xy} & R_{xz} \\ R_{yx} & R_{yy} & R_{yz} \\ R_{zx} & R_{zy} & R_{zz} \end{pmatrix} = \begin{pmatrix} \cos\phi & -\sin\phi & 0 \\ \sin\phi & \cos\phi & 0 \\ 0 & 0 & 1 \end{pmatrix} \tag{17}$$

The relationship between the macroscopic susceptibility tensor elements and the microscopic polarizability tensor terms is,

$$\chi_{IJK} = \sum_{ijk} \langle R_{Ii} R_{Jj} R_{Kk} \rangle \beta_{ijk} \tag{18}$$

Accordingly, the 14 non-zero elements in Table IV for z-cut a-quartz crystal are derived and listed in Table V.

Using the field vector projections in Table III, the non-zero macroscopic susceptibility terms, and the expressions in the Table V, the following effective susceptibility terms in the 8 polarization combinations

DOI:10.1063/1674-0068/29/cjcp1512248

are derived for the XP-SFG-VS with z-cut α-quartz (Eq.(19)−Eq.(28)). In these expressions, the red terms are contributions from the achiral terms of the quartz unit cell, and the black are contribution from the chiral terms.

$$\begin{aligned}\chi_{\rm sss} &= -L_{XX}(\omega)L_{YY}(\omega_1)L_{YY}(\omega_2)\sin\gamma\cdot\chi_{XYX}+\\ &\quad L_{YY}(\omega)L_{YY}(\omega_1)L_{YY}(\omega_2)\cos\gamma\cdot\chi_{YYX}\\ &= -L_{XX}(\omega)L_{YY}(\omega_1)L_{YY}(\omega_2)\sin\gamma\cdot\beta_{xxx}\\ &\quad \sin 3\phi - L_{YY}(\omega)L_{YY}(\omega_1)L_{YY}(\omega_2)\cos\gamma\cdot\\ &\quad \beta_{xxx}\cos 3\phi \qquad (19)\\ \chi_{\rm ssp} &= -L_{XX}(\omega)L_{YY}(\omega_1)L_{XX}(\omega_2)\sin\gamma\cos\beta_2\cdot\\ &\quad \chi_{XYY} - L_{XX}(\omega)L_{YY}(\omega_1)L_{ZZ}(\omega_2)\sin\gamma\sin\beta_2\cdot\\ &\quad \chi_{XYZ}+L_{YY}(\omega)L_{YY}(\omega_1)L_{XX}(\omega_2)\cos\gamma\cos\beta_2\cdot\\ &\quad \chi_{YYY}\\ &= +L_{XX}(\omega)L_{YY}(\omega_1)L_{XX}(\omega_2)\sin\gamma\cos\beta_2\cdot\\ &\quad \beta_{xxx}\cos 3\phi - L_{XX}(\omega)L_{YY}(\omega_1)L_{ZZ}(\omega_2)\cdot\\ &\quad \sin\gamma\sin\beta_2\beta_{xyz}-L_{YY}(\omega)L_{YY}(\omega_1)L_{XX}(\omega_2)\cdot\\ &\quad \cos\gamma\cos\beta_2\cdot\beta_{xxx}\sin 3\phi \qquad (20)\\ \chi_{\rm sps} &= -L_{XX}(\omega)L_{XX}(\omega_1)L_{YY}(\omega_2)\sin\gamma\cos\beta_1\cdot\\ &\quad \chi_{XXX}+L_{YY}(\omega)L_{XX}(\omega_1)L_{YY}(\omega_2)\cdot\\ &\quad \cos\gamma\cos\beta_1\chi_{YXX}+L_{YY}(\omega)L_{ZZ}(\omega_1)L_{YY}(\omega_2)\cdot\\ &\quad \cos\gamma\sin\beta_1\cdot\chi_{YZX} \qquad (21)\\ &= -L_{XX}(\omega)L_{XX}(\omega_1)L_{YY}(\omega_2)\sin\gamma\cos\beta_1\cdot\\ &\quad \beta_{xxx}\cos 3\phi\cdot\beta_{xxx}\cos 3\phi+L_{YY}(\omega)L_{XX}(\omega_1)\cdot\\ &\quad L_{YY}(\omega_2)\cos\gamma\cos\beta_1\cdot\beta_{xxx}\sin 3\phi - L_{YY}(\omega)\\ &\quad L_{ZZ}(\omega_1)L_{YY}(\omega_2)\cos\gamma\sin\beta_1\cdot\beta_{xyz} \qquad (22)\\ \chi_{\rm pss} &= -L_{XX}(\omega)L_{YY}(\omega_1)L_{YY}(\omega_2)\cos\gamma\cos\beta\cdot\\ &\quad \chi_{XYX} - L_{YY}(\omega)L_{YY}(\omega_1)L_{YY}(\omega_2)\cdot\\ &\quad \sin\gamma\cos\beta\cdot\chi_{YYX} \qquad (23)\\ &= -L_{XX}(\omega)L_{YY}(\omega_1)L_{YY}(\omega_2)\cos\gamma\cos\beta\cdot\\ &\quad \beta_{xxx}\sin 3\phi+L_{YY}(\omega)L_{YY}(\omega_1)L_{YY}(\omega_2)\cdot\\ &\quad \sin\gamma\cos\beta\cdot\beta_{xxx}\cos 3\phi \qquad (24)\\ \chi_{\rm pps} &= -L_{XX}(\omega)L_{XX}(\omega_1)L_{YY}(\omega_2)\cos\gamma\cos\beta\cdot\\ &\quad \cos\beta_1\cdot\chi_{XXX}-L_{YY}(\omega)L_{XX}(\omega_1)L_{YY}(\omega_2)\cdot\\ &\quad \sin\gamma\cos\beta\cos\beta_1\cdot\chi_{YXX}-L_{YY}(\omega)L_{ZZ}(\omega_1)\cdot\\ &\quad L_{YY}(\omega_2)\sin\gamma\cos\beta\sin\beta_1\cdot\chi_{YZX}\\ &= -L_{XX}(\omega)L_{XX}(\omega_1)L_{YY}(\omega_2)\cos\gamma\cos\beta\cdot\\ &\quad \cos\beta_1\cdot\beta_{xxx}\cos 3\phi - L_{YY}(\omega)L_{XX}(\omega_1)\cdot\\ &\quad L_{YY}(\omega_2)\sin\gamma\cos\beta\cos\beta_1\cdot\beta_{xxx}\sin 3\phi+\\ &\quad L_{YY}(\omega)L_{ZZ}(\omega_1)L_{YY}(\omega_2)\cdot\\ &\quad \sin\gamma\cos\beta\sin\beta_1\cdot\beta_{xyz} \qquad (25)\\ \chi_{\rm psp} &= -L_{XX}(\omega)L_{YY}(\omega_1)L_{XX}(\omega_2)\cos\gamma\cos\beta\cdot\\ &\quad \cos\beta_2\cdot\chi_{XYY}-L_{XX}(\omega)L_{YY}(\omega_1)L_{ZZ}(\omega_2)\cdot\\ &\quad \cos\gamma\cos\beta\sin\beta_2\cdot\chi_{XYZ}-L_{YY}(\omega)L_{YY}(\omega_1)\cdot\\ &\quad L_{XX}(\omega_2)\sin\gamma cos\beta\cos\beta_2\cdot\chi_{YYY}\\ &= +L_{XX}(\omega)L_{YY}(\omega_1)L_{XX}(\omega_2)\cos\gamma\cos\beta\cos\beta_2\cdot\\ &\quad \beta_{xxx}\cos 3\phi - L_{XX}(\omega)L_{YY}(\omega_1)L_{ZZ}(\omega_2)\cdot\\ &\quad \cos\gamma\cos\beta\sin\beta_2\cdot\beta_{xyz}+L_{YY}(\omega)L_{YY}(\omega_1)\cdot\\ &\quad L_{XX}(\omega_2)\sin\gamma\cos\beta\cos\beta_2\cdot\beta_{xxx}\sin 3\phi \qquad (26)\\ \chi_{\rm spp} &= -L_{XX}(\omega)L_{XX}(\omega_1)L_{XX}(\omega_2)\sin\gamma\cos\beta_1\cdot\\ &\quad \cos\beta_2\cdot\chi_{XXY}+L_{YY}(\omega)L_{XX}(\omega_1)\cdot\\ &\quad L_{XX}(\omega_2)\cos\gamma\cos\beta_1\cos\beta_2\cdot\chi_{YXY}+\\ &\quad L_{YY}(\omega)L_{XX}(\omega_1)L_{ZZ}(\omega_2)\cdot\\ &\quad \cos\gamma\cos\beta_1\sin\beta_2\cdot\chi_{YXZ}\\ &= -L_{XX}(\omega)L_{XX}(\omega_1)L_{XX}(\omega_2)\sin\gamma\cos\beta_1\cdot\\ &\quad \cos\beta_2\cdot\beta_{xxx}\sin 3\phi - L_{YY}(\omega)L_{XX}(\omega_1)\cdot\\ &\quad L_{XX}(\omega_2)\cos\gamma\cos\beta_1\cos\beta_2\cdot\beta_{xxx}\cos 3\phi-\\ &\quad L_{YY}(\omega)L_{XX}(\omega_1)L_{ZZ}(\omega_2)\cdot\\ &\quad \cos\gamma\cos\beta_1\sin\beta_2\cdot\beta_{xyz} \qquad (27)\\ \chi_{\rm ppp} &= -L_{XX}(\omega)L_{XX}(\omega_1)L_{XX}(\omega_2)\cos\gamma\cos\beta\cdot\\ &\quad \cos\beta_1\cos\beta_2\cdot\chi_{XXY}-L_{XX}(\omega)L_{ZZ}(\omega_1)\cdot\\ &\quad L_{XX}(\omega_2)\cos\gamma\cos\beta\sin\beta_1\cos\beta_2\cdot\chi_{XZY}-\\ &\quad L_{YY}(\omega)L_{XX}(\omega_1)L_{XX}(\omega_2)\sin\gamma\cos\beta\cdot\\ &\quad \cos\beta_1\cos\beta_2\cdot\chi_{YXY}-L_{YY}(\omega)L_{XX}(\omega_1)\cdot\\ &\quad L_{ZZ}(\omega_2)\sin\gamma\cos\beta\cos\beta_1\sin\beta_2\cdot\chi_{YXZ}\\ &= -L_{XX}(\omega)L_{XX}(\omega_1)L_{XX}(\omega_2)\cos\gamma\cos\beta\cdot\\ &\quad \cos\beta_1\cos\beta_2\cdot\beta_{xxx}\sin 3\phi - L_{XX}(\omega)\cdot\\ &\quad L_{ZZ}(\omega_1)L_{XX}(\omega_2)\cos\gamma\cos\beta\sin\beta_1\cos\beta_2\cdot\\ &\quad \beta_{xyz}+L_{YY}(\omega)L_{XX}(\omega_1)L_{XX}(\omega_2)\cdot\\ &\quad \sin\gamma\cos\beta\cos\beta_1\cos\beta_2\cdot\beta_{xxx}\cos 3\phi+\\ &\quad L_{YY}(\omega)L_{XX}(\omega_1)L_{ZZ}(\omega_2)\sin\gamma\cdot\\ &\quad \cos\beta\cos\beta_1\sin\beta_2\cdot\beta_{xyz} \qquad (28)\end{aligned}$$

Here, Eq.(19)−Eq.(28) for the XP-SFG-VS on z-cut α-quartz can also be compared with the corresponding terms in the co-propagation case in the co-planar geometry in the literature [14, 22, 23, 39]. It is similar to the C_∞ surface discussed above, there is no longer a pure achiral term in the XP-SFG-VS expressions. However, the case for the D_3 symmetry is apparently much more complicated than the case for the C_∞ symmetry. For example, in Eq.(20), there are contributions from both the $\beta_{xxx}\sin 3\phi$ and $\beta_{xxx}\cos 3\phi$ terms to the ssp susceptibility term, instead of only the $\beta_{xxx}\cos 3\phi$ term in the case for co-propagation case. To evaluate the relative contribution and overall azimuthal angle dependence from the sum of these two mutually excluding terms as well as the chiral term can be quite complicated, especially for the phonon modes or quartz in the 750−1300 $\rm cm^{-1}$ region, as shown in previous studies by Liu and Shen [40, 41]. By applying the small $\sin\gamma$ approximation, one can find that the ssp term in Eq.(20) is dominated by the $\beta_{xxx}\sin 3\phi$ azimuthal angle dependence, instead of the $\beta_{xxx}\cos 3\phi$ term as in the ssp term in the co-propagation case in the co-planar geometry [14]. However, how good this approximation is depends also on the Fresnel factors at specific frequencies that are resonant with specific vibrational modes [40, 41]. Nevertheless, the full expressions as presented in the

DOI:10.1063/1674-0068/29/cjcp1512248

Eq.(19)−Eq.(28) provide the frameworks to quantitatively evaluate these factors.

One final note to the Eq.(19) to Eq.(28) is that the Fresnel factors in the SFG literature are usually defined by assuming the substrate is without birefringence. Actually this is not always true and may result complications in the evaluation of the overall effective susceptibility in these equations. For example, for z-cut α-quartz, since its z axis is the optical axis, any incident or outgoing beam with polarization in the incident or outgoing plane, *i.e.* the p polarization, is the ordinary ray, while the beam with polarization perpendicular to the incident or outgoing plane, *i.e.* the s polarization, is the extraordinary ray. When there is birefringence, the refractive indexes of the ordinary and extraordinary rays are different. Thus the Fresnel factors needs to be calculated accordingly for the s and p polarization, respectively. Even though the birefringence of z-cut α-quartz is known to be small (Δn=n_e−n_o≈0.009 in the visible region) [42], its birefringence can still be observed if the SFG measurement is done accurately. The effect is to be much larger for materials such as rutile TiO_2 (Δn=n_e−n_o≈0.28 in the visible region) or anatase TiO_2 (Δn=n_e−n_o≈0.17 in the visible region) [42], whose surfaces are important for studying photocatalytic reactions and have been extensively studies using SFG-VS [31, 43, 44]. These effects can be more significant when dealing with their low frequency modes. Further work regarding these effects in the SFG-VS in both the XP-SFG-VS and the co-planar geometry SFG-VS measurements is warranted.

III. EXPERIMENTS

To demonstrate the XP-SFG-VS does work, the XP-SFG-VS spectra of a few model surfaces are measured using both recently developed sub 1-cm^{-1} high-resolution broadband SFG-VS (HR-BB-SFG-VS) with a narrow 800 nm visible beam (resolution about 0.6 cm^{-1}). Data for the z-cut α-quartz in the 1000−1280 cm^{-1} region from the high-resolution XP-SFG-VS are also compared with the co-propagation geometry data from a commercially available picosecond scanning SFG-VS spectrometer with a 532.1 nm visible beam (EKSPLA, Inc., resolution about 6 cm^{-1}). The detailed descriptions of the HR-BB-SFG-VS spectrometer [13, 14, 45] and the picosecond scanning SFG-VS spectrometer [27, 46, 47] can be found in our previous publications.

To achieve XP-SFG-VS measurement, the IR beam is redirected with IR optical mirrors into the cross-polarization. In all the experiments, we choose the simplest XP-SFG-VS case with the same incident angles for the visible and the IR beams in their respective incident plane, *i.e.* β_1=β_2 as defined in Fig.1. The SFG detection angles followed the calculated β and γ values as in the Table II.

Neat dimethyl sulfoxide (Sigma-Aldrich 99.9%) and cyclohexanol (Sigma-Aldrich 99%) liquids wereused as received. The air/DMSO interface was prepared by pouring 8 mL into ateflon Petry dish which was carefully cleaned with a Nochromix (Godax Laboratories, Inc) and sulfuric acidmixture, rinsed with Millipore water (18 MΩ·cm, Millipore Corp.), and followed by 12 min of UV/ozone cleaning. When making the cyclohexanol on vapor/z-cut α-quartz, aright-handed z-cut α-quartz with square shape (size 12.7 mm×12.7 mm×5 mm, Conex System Technology) was placed in a Teflon dish about 8 mm deep, and a drop of cyclohexanol aqueous solution (0.32 mol/L, with 18 MΩ·cm Millipore water) was placed at the bottom of the Teflon dish, and the dish was covered with an ozone plasma cleaned CaF_2 window (5 cm diameter×4 mm thickness). The cyclohexanol evaporated and was adsorbed on the quartz surface.

The SFG measurement in the 2800−3050 cm^{-1} range usually takes 5 min acquisition time, and the signal was normalized to the SFG profile of a thick z-cut α-quartz (size 12.7 mm×12.7 mm×5 mm) at azimuthal angle of ϕ=0°, as in all our previous HR-BB-SFG-VS measurement [13, 14]. The SFG measurement in the 1000−1280 cm^{-1} region on the z-cut α-quartz surface usually take 60 s acquisition time, and the signal is normalized to the SFG profile of a ZnS plate (Cleatran, ISP Optics, Inc.). This is because in this lower frequency IR region, z-cut α-quartz is no longer spectroscopically flat. So in the broadband SFG measurement the IR spectral profile was measured by the spectroscopically flat ZnS in this region for normalization. While for the scanning SFG measurement, the signal intensity was normalized directly to the visible and IR power. So the absolute value of the two sets of data cannot be directly compared without additional intensity calibration.

All experiments were performed with a freshly poured sample. All experiments were performed at room temperature of 22±2 °C.

IV. RESULTS AND DISCUSSION

Here we present the realization of the reflective XP-SFG-VS measurement on the air/DMSO interface and cyclohexanol on the vapor/z-cut α-quartz surface in the C−H stretching vibration region, *i.e.* in 2800−3050 cm^{-1}, and the air/z-cut α-quartz surface in the 1000−1280 cm^{-1} phonon mode region. These results show the feasibility of the XP-SFG-VS and also provided validation of the formulation presented above.

The air/DMSO interface is one of the benchmark achiral interfaces for HR-BB-SFG-VS measurement [13, 48]. Figure 4 shows the ssp and ppp spectra of the air/DMSO interface in the XP-SFG-VS with β_1=β_2=45°. In the measurement, the dihedral angle between the SFG and IR planes is fixed at γ=13°, showing the validity of the values calculated in the Ta-

DOI:10.1063/1674-0068/29/cjcp1512248

ble II. One can see that the spectral lineshapes in the ssp and ppp polarization combinations are similar to the lineshapes of the reported SFG-VS HR-BB-SFG-VS spectra in the co-propagation co-planar geometry with β_1=45° and β_2=55° [13, 49], except for that the relative ssp and ppp intensity of the sharp ∼2920 cm^{-1} peak is slightly different. These results can be readily understood by comparing the ssp and ppp effective susceptibility expressions, *i.e.* Eq.(9) and Eq.(14), respectively, for the XP-SFG-VS, and the ssp and ppp expressions for the co-propagation case in the literature [11]. The achiral ssp terms of the rotationally isotropic liquid surface in the two geometries are both from the contribution from a single the YYZ macroscopic susceptibility term. However, the ppp term in the XP-SFG-VS in this case are with contributions from the three achiral XXZ, YZY and ZZZ terms; while in the co-propagation co-planar case the ppp term are with contributions from the four achiral XXZ, XZX, ZXX and ZZZ terms. Quantitative analysis of the XP-SFG-VS from the rotationally isotropic chiral and achiral surfaces should follow the Eq.(8) to Eq.(14).

In the experiment we noticed that the ssp signal intensities in the XP-SFG-VS and in the co-propagation co-planar measurement are at similar signal levels for the air/DMSO interface. This fact can be readily comprehended as in the XP-SFG-VS the ssp term is $L_{YY}(\omega)L_{YY}(\omega_1)L_{ZZ}(\omega_2)\cos\gamma\sin\beta_2\times\chi_{YYZ}$ (Eq.(9)), while in the co-propagation co-planar geometry, the ssp term is $L_{YY}(\omega)L_{YY}(\omega_1)L_{ZZ}(\omega_2)\sin\beta_2\times\chi_{YYZ}$ [11]. The only difference between them is the factor of $\cos\gamma$, which is close to unity as the value of γ is usually small (Table II). The same is also true when comparing the SFG-VS signal from the thick z-cut α-quartz crystal surface in both geometries, where a single reflection from the quartz crystal region that satisfies phase match condition was responsible for the generated SFG signal. However, the XP-SFG-VS signal from the thin z-cut α-quartz crystal (about 200 μm thickness) is usually 30 times smaller than that with the co-propagation co-planar geometry. The reason for this is that there are interferences of SFG-VS signals generated from multiple reflections of the visible and IR beams in the thin quartz crystal in the co-propagation co-planar geometry; while in the cross-propagation geometry such multiple reflection interference phenomenon is significantly reduced as the visible and IR beams are going different directions after the initial overlapping point. Therefore, one advantage for the XP-SFG-VS is to avoid the complication from such multiple interferences from molecular layers adsorbed on thin substrate surfaces.

It has been shown recently that the effective susceptibility from the quartz crystal surface contains the bulk contribution of the nonlinear quartz crystal and the surface contribution of the adsorbed molecular layer. Because the bulk SFG response has an intrinsic shift of optical phase by $\pi/2$ from that of the surface response, the overall SFG signal from this interface provided a

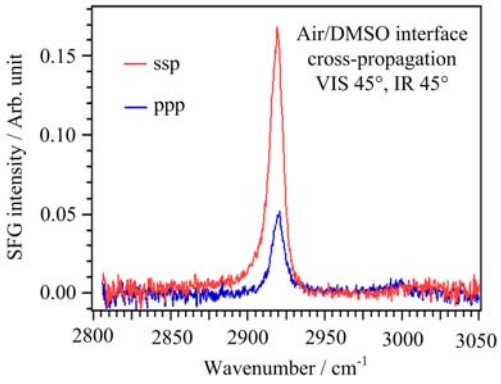

FIG. 4 HR-BB-SFG-VS in the cross-propagation geometry for air/DMSO interface in the range of 2800−3050 cm^{-1}.

direct measurement of the phase-resolved spectra of the adsorbed molecular layer, as long as the bulk response is spectroscopically flat in the frequency region [14]. The interference pattern depends on the relative phase between the quartz bulk term and the orientation of the molecular groups on the interface. It has been known that if the CH_3 or CH_2 dipole direction is pointing away from the surface, the absolute phase of the imaginary part of their symmetric stretching modes should be positive [14]. Therefore, in the Fig.5, the two positive peaks (∼2860 and ∼2945 cm^{-1}) measured with the quartz crystal azimuthal angle the ϕ=0° suggests that the quartz term at ϕ=0° is positive in phase; and the quartz term with ϕ=180° is negative in phase, and the interference pattern are with negative peaks. This results put the ssp response of the z-cut α-quartz in the XP-SFG-VS to be opposite in phase (sign) to that of the co-propagation planar geometry [14]. Nevertheless, these results can be easily understood with the respective expressions of the ssp terms for the z-cut α-quartz crystal surface. In the XP-SFG-VS case with Eq.(20), the quartz ssp term at ϕ=0° is dominated by the term $L_{XX}(\omega)L_{YY}(\omega_1)L_{XX}(\omega_2)\sin\gamma\cos\beta_2\cdot\beta_{xxx}$ and it changes sign at ϕ=180°. It is therefore positive at ϕ=0° and negative at ϕ=180°. While in the co-propagation planar geometry case, it has been known that the quartz ssp term at ϕ=0° is dominated by the term $-L_{YY}(\omega)L_{YY}(\omega_1)L_{XX}(\omega_2)\cos\beta_2\cdot\beta_{xxx}$ and it changes sign at ϕ=180°. Therefore, it is negative at ϕ=0° and positive at ϕ=180° for the co-propagation co-planar case. Therefore, the phase-resolved XP-SFG-VS results in Fig.5 confirmed the validity of the formulations for z-cut α-quartz in the XP-SFG-VS. Such differences between the XP-SFG-VS and co-propagation co-planar SFG-VS needs to be carefully examined when making phase resolved measurements using the two SFG-VS geometries.

Figure 6 shows the high-resolution broadband XP-SFG-VS measurement of z-cut α-quartz crystal surface in the 1000−1280 cm^{-1} region in the ssp, ppp and spp polarization combinations. These spectra can also be

DOI:10.1063/1674-0068/29/cjcp1512248

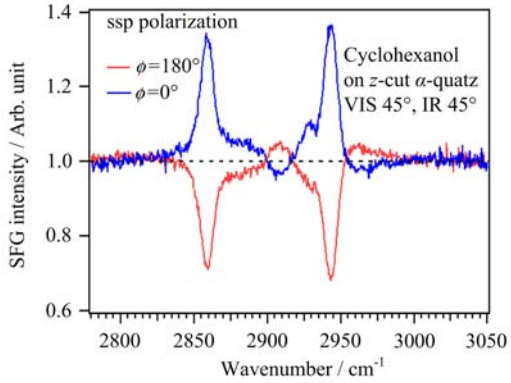

FIG. 5 HR-BB-SFG-VS interference spectra of cyclohexanol on vapor/z-cut α-quartz crystal interface in the cross-propagation. The interference pattern has opposite sign in comparison to the co-propagation co-planar geometry.

compared with the ssp and ppp spectra in the same region measured with the co-propagation co-planar SFG-VS using a picosecond scanning SFG spectrometer. One can see that the main spectral features in the XP-SFG-VS and the co-propagation co-planar SFG-VS spectra are consistent with each other. The two apparent peaks at about 1065 and 1160 cm^{-1} are known from the bulk phonon modes and have been studied extensively by Shen and co-workers previously [40, 41]. Here, we only presented the proof-of-principle data with azimuthal angle ϕ=0° with XP-SFG-VS. The spp spectral intensity at ϕ=0° is significantly stronger than that of the ssp and ppp spectra. This can only happen in the XP-SFG-VS but not in the co-propagation co-planar geometry [14, 40, 41]. These differences can be quantitatively understood with the formulations for the XP-SFG-VS presented in this work and for the co-propagation co-planar SFG-VS previously [14, 39–41].

V. CONCLUSION

In this work, we presented the theoretical formulation of the cross-propagation non-planar SFG-VS (XP-SFG-VS) with surface or interface with both C_∞ and D_3 symmetries. We also presented experimental results from XP-SFG-VS measurement on the air/DMSO (dimethyl sulfoxide) interface, adsorbed cyclohexanol layer on the vapor/z-cut α-quartz surface in the C−H stretching vibration region, *i.e.* in 2800−3050 cm^{-1}, and the air/z-cut α-quartz surface in the 1000−1280 cm^{-1} phonon mode region. The similarities and differences in the XP-SFG-VS and the commonly used co-propagation co-planar geometry SFG-VS are also compared and examined.

Because of the momentum conservation condition, the visible, IR and SFG beams can no longer be in the same incident plane in XP-SFG-VS. As the result, the expressions for the effective susceptibility in different polarization combinations in XP-SFG-VS are

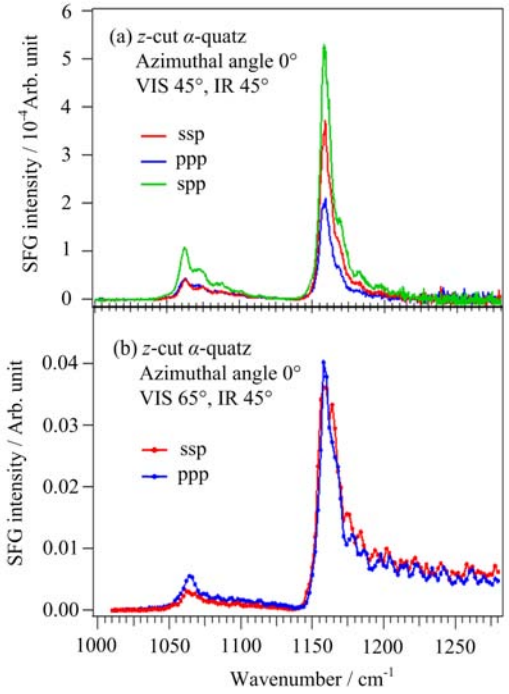

FIG. 6 Measurement of the phonon modes of the z-cut α-quartz crystal surface in the 1000−1280 cm^{-1}. (a) HR-BB-SFG-VS in the cross-propagation geometry. The SFG intensity was normalized to SFG signal from a ZnS plate. (b) Scanning SFG-VS in the co-propagation geometry. The SFG intensity was normalized to the intensity of the visible and IR power intensity monitored with a pyroelectric detector.

more complicated than their counterparts in the co-planar SFG-VS. However, in this work, we showed how these expression can be derived in detail and how experimental data can be understood using the formulations. It turned out that the XP-SFG-VS formulation with perpendicular visible and IR incident planes and equal incident angles is the simplest case in the non- co-planar SFG-VS. Using such conditions, qualitative understanding and quantitative analysis of XP-SFG-VS data can be achieved in a relatively less complicated fashion.

The ultimate purpose of this work on the XP-SFG-VS is to provide a practical solution for the limitations on the window material choices in the co-planar geometry SFG-VS to study the surfaces in the enclosed vacuum or pressure chamber. SFG-VS measurement on these surfaces is most useful for the surface sciences and fundamental catalysis studies, where both the vibrational spectra of the adsorbed molecular layers and the lower IR frequency vibrations of the substrate surface are of interest. We hope the theoretical and experimental exercises presented in this work shall be helpful in designing vacuum and pressure chambers for broader applications of SFG-VS measurements in the surface sciences, material sciences, catalytic sciences, as well as low-temperature molecular sciences, *etc.*

DOI:10.1063/1674-0068/29/cjcp1512248

VI. ACKNOWLEDGEMENTS

Hong-Fei Wang thanks Professor Ze-feng Ren and Wei-tao Liu for discussions that later led him to consider the idea of XP-SFG-VS. Li Fu and Shun-li Chen thank Zizwe Chase for experimental assistance. Wei Gan thanks for the support from the "1000 Talent Program" (The Recruitment Program of Global Experts). Part of this work was conducted at the William R. Wiley Environmental Molecular Sciences Laboratory (EMSL), a national scientific user facility located at the Pacific Northwest National Laboratory (PNNL) and sponsored by the Department of Energy's Office of Biological and Environmental Research (BER). Li Fu is the William R. Wiley postdoc fellow at EMSL. Shun-li Chen, who is an assistant professor at the Xinjiang Technical Institute of Physics & Chemistry of the Chinese Academy of Sciences, is an Alternate Sponsored Fellow at PNNL working in EMSL during this work.

[1] H. W. K. Tom, *Studies of Surfaces Using Optical Second-harmonic Generation*, Ph.D. Dissertation, Berkeley: University of California, (1984).
[2] Y. R. Shen, Nature **337**, 519 (1989).
[3] K. B. Eisenthal, Chem. Rev. **96**, 1343 (1996).
[4] G. A. Somorjai and G. Rupprechter, J. Phys. Chem. B **103**, 1623 (1999).
[5] M. Buck and M. Himmelhaus, J. Vacu. Sci. Tech. A **19**, 2717 (2001).
[6] C. S. Tian and Y. R. Shen, Surf. Sci. Rep. **69**, 105 (2014).
[7] E. C. Y. Yan, L. Fu, Z. Wang, and W. Liu, Chem. Rev. **114**, 8471 (2014).
[8] H. Arnolds and M. Bonn, Surf. Sci. Rep. **65**, 45 (2010).
[9] Y. R. Shen, Annu. Rev. Phys. Chem. **64**, 129 (2013).
[10] H. F. Wang, W. Gan, R. Lu, Y. Rao, and B. H. Wu, Int. Rev. Phys. Chem. **24**, 191 (2005).
[11] H. F. Wang, L. Velarde, W. Gan, and L. Fu, Annu. Rev. Phys. Chem. **66**, 189 (2015).
[12] L. Velarde and H. F. Wang, Phys. Chem. Chem. Phys. **15**, 19970 (2013).
[13] L. Velarde, X. Y. Zhang, Z. Lu, A. G. Joly, Z. M. Wang, and H. F. Wang, J. Chem. Phys. **135**, 241102 (2011).
[14] L. Fu, S. L. Chen, and H. F. Wang, J. Phys. Chem. B DOI:101021/acs.jpcb.5b07780.
[15] R. R. Feng, Y. Guo, R. Lu, L. Velarde, and H. F. Wang, J. Phys. Chem. A **115**, 6015 (2011).
[16] R. E. Pool, J. Versluis, E. H. G. Backus, and M. Bonn, J. Phys. Chem. B **115**, 15362 (2011).
[17] S. Yamaguchi, J. Chem. Phys. **143**, 034202 (2015).
[18] S. Nihonyanagi, R. Kusaka, K. I. Inoue, A. Adhikari, S. Yamaguchi, and T. Tahara, J. Chem. Phys. **143**, 124707 (2015).
[19] Y. R. Shen, *The Principles of Nonlinear Optics*, New York: Wiley-Interscience, (1984).
[20] Y. R. Shen, *Fundamentals of Sum-Frequency Spectroscopy*, Cambridge University Press, (2016).
[21] C. D. Bain, P. B. Davies, T. H. Ong, R. N. Ward, and M. A. Brown, Langmuir **7**, 1563 (1991).
[22] V. Ostroverkhov, G. A. Waychunas, and Y. R. Shen, Chem. Phys. Lett. **386**, 144 (2004).
[23] V. Ostroverkhov, G. A. Waychunas, and Y. R. Shen, Phys. Rev. Lett. **94**, 046102 (2005).
[24] L. F. Scatena, M. G. Brown, and G. L. Richmond, Science **292**, 908 (2001).
[25] C. T. Williams and D. A. Beattie, Surf. Sci. **500**, 545 (2002).
[26] S. Schrodle, F. G. Moore, and G. L. Richmond, J. Phys. Chem. C **111**, 10088 (2007).
[27] Z. Lu, A. Karakoti, L. Velarde, W. Wang, P. Yang, S. Thevuthasan, and H. F. Wang, J. Phys. Chem. C **117**, 24329 (2013).
[28] P. Mukherjee, A. Lagutchev, and D. D. Dlott, J. Electrochem. Soc. **159**, A244 (2012).
[29] F. Zaera, Chem. Rev. **112**, 2920 (2012).
[30] J. P. R. Symonds, H. Arnolds, and D. A. King, J. Phys. Chem. B **108**, 14311 (2004).
[31] R. R. Feng, A. A. Liu, S. Liu, J. Shi, R. Zhang, and Z. Ren, J. Chem. Phys. C **119**, 9798 (2015).
[32] Y. Tong, K. Cai, M. Wolf, and R. K. Campen, Catal. Today **260**, 66 (2016).
[33] Y. Tong, J. Wirth, H. Kirsch, M. Wolf, P. Saalfrank, and R. K. Campen, J. Chem. Phys. **142**, 054704 (2015).
[34] Y. R. Shen, *Surface Spectrocopy by Nonlinear Optics, in Frontiers in Laser Spectroscopy*, T. W. Hansch and M. Inguscio, Eds., Verenna, Italy: International School of Physics-Enrico Fermi, 139 (1994).
[35] X. Zhuang, P. B. Miranda, D. Kim, and Y. R. Shen, Phys. Rev. B **59**, 12632 (1999).
[36] N. Bloembergen and P. S. Pershan, Phys. Rev. **128**, 606 (1962).
[37] N. Bloembergen, *Nonlinear Optics*, Benjamin: Lecture Note and Reprint Volume, (1965).
[38] G. R. Crane and J. G. Bergman, J. Chem. Phys. **64**, 27 (1976).
[39] D. K. Hore, M. Y. Hamamoto, and G. L. Richmond, J. Chem. Phys. **121**, 12589 (2004).
[40] W. T. Liu and Y. R. Shen, Phys. Rev. Lett. **101**, (2008).
[41] W. T. Liu and Y. R. Shen, Phys. Rev. B **78**, 024302 (2008).
[42] M. J. Weber, *Handbook of Optical Materials*, Taylor & Francis, (2002).
[43] A. A. Liu, S. Liu, R. Zhang, and Z. Ren, J. Chem. Phys. C **119**, 23486 (2015).
[44] S. Liu, A. A. Liu, B. Wen, R. Zhang, C. Zhou, L. M. Liu, and Z. Ren, J. Phys. Chem. Lett. **6**, 3327 (2015).
[45] L. Velarde and H. F. Wang, J. Chem. Phys. **139**, 084204 (2013).
[46] R. Lu, W. Gan, B. H. Wu, H. Chen, and H. F. Wang, J. Phys. Chem. B **108**, 7297 (2004).
[47] R. Lu, W. Gan, B. H. Wu, Z. Zhang, Y. Guo, and H. F. Wang, J. Phys. Chem. B **109**, 14118 (2005).
[48] L. Fu, Y. Zhang, Z. H. Wei, and H. F. Wang, Chirality **26**, 509 (2014).
[49] L. Velarde, Z. Lu, and H. F. Wang, Chin. J. Chem. Phys. **26**, 710 (2013).

DOI:10.1063/1674-0068/29/cjcp1512248